Structural and Electrical Characterization of the Novel $SrCo_{0.9}Sb_{0.1}O_{3-\delta}$ Perovskite: Evaluation as a Solid Oxide Fuel Cell Cathode Material

A. Aguadero,*,† C. de la Calle,‡ J. A. Alonso,‡ M. J. Escudero,† M. T. Fernández-Díaz,§ and L. Daza†,||

Centro de Investigaciones Energéticas Mediambientales y Tecnológicas (CIEMAT), Avenida Complutense 22, 28040 Madrid, Spain, Instituto de Ciencia de Materiales de Madrid, CSIC, Cantoblanco, 28049 Madrid, Spain, Institute Laue-Langevin (ILL) 156X, F-38042 Grenoble Cedex 9, France, and Instituto de Catálisis y Petroleoquímica, CSIC, Cantoblanco, 28049 Madrid, Spain

Received July 12, 2007. Revised Manuscript Received September 20, 2007

A novel perovskite oxide with the title composition has been prepared by soft-chemistry procedures followed by thermal treatments at 1000 °C. This polycrystalline sample has been characterized by temperature-dependent neutron powder diffraction (NPD), thermal analysis, electrical conductivity, and thermal expansion measurements, in order to evaluate its potential use as a mixed electronic–ionic conductor in intermediate-temperature solid oxide fuel cells (IT-SOFCs). At room temperature (RT), the sample adopts a tetragonal superstructure of perovskite with $a = a_0$, $c = 2a_0$ ($a_0 \approx 3.9$ Å) defined in the *P4/mmm* space group. Co and Sb are distributed at random over the octahedral positions of the perovskite; flattened and elongated $(Co,Sb)O_6$ octahedra alternate along the *c* axis, sharing corners in a three-dimensional array (3C-like structure). The refinement of the oxygen occupancy factors yields the crystallographic formula $SrCo_{0.9}Sb_{0.1}O_{2.73(4)}$; the oxygen vacancies are located at the equatorial O2 and O3 atoms, in alternating layers with different occupancy. O3 atoms exhibit, at RT, large thermal factors of 5.3 $Å^2$, suggesting a considerable mobility. This structure is stable up to 500 °C; between 500 and 700 °C, an order–disorder phase transition takes place to give a fully disordered simple-cubic perovskite with $a = a_0$ (space group $Pm\bar{3}m$); this structure is shown to be stable up to 940 °C from NPD data. This is a second-order nonreconstructive transition, which is not observed at the differential thermal analysis curves, although it is probably responsible for a subtle change of slope at 650 °C in the thermal expansion curve. The thermal evolution of the electrical conductivity exhibits a maximum of 300 $S \cdot cm^{-1}$ at 400 °C; above this electronic transition, the conductivity regularly decreases, but it is still well above the required 100 $S \cdot cm^{-1}$ in the temperature region 650–850 °C corresponding to the working regime of a IT-SOFC.

Introduction

One of the major improvements required for the commercialization of solid oxide fuel cell (SOFC) devices is the reduction of the operating temperature and, therefore, the cost of the materials and maintenance of the cell without detriment of the cell efficiency. In this regard, many efforts have been focused on the development of new cell materials with better performance (lower resistance) at lower temperatures (650–850 °C) that also fulfill with the cell requirements. In the field of cathode materials, many efforts are being engaged to prepare and characterize oxides with mixed ionic–electronic conductivity (MIEC)[1,2] to be used in intermediate-temperature SOFCs (IT-SOFCs). The use of MIEC improves the kinetic reactions of the oxygen reduction because of the enhancement of the active area from the triple-phase boundary electrode–electrolyte–air to a double-interphase electrode (MIEC)–air. [3,4] In this case, MIEC materials provide not only the electrons for the reduction of oxygen, like the habitual cathode SOFC material LSM ($La_{0.8}Sr_{0.2}MnO_{3-\delta}$) at high temperature, but also the ionic conduction required to ensure the transport of the formed oxygen ions between the double interphase and the electrolyte, thus allowing the reduction of the operation temperature.

The family of compounds with perovskite structure containing Co and Sr has received considerable attention as oxygen-permeating membranes, sensors, or cathodes for SOFCs because of their high oxygen permeability values, which are 1 or 2 orders of magnitude greater than that of yttria-stabilized zirconia.[5]

* Corresponding author. E-mail: ainara.aguadero@ciemat.es.
† CIEMAT.
‡ Instituto de Ciencia de Materiales de Madrid, CSIC.
§ Institute Laue-Langevin.
|| Instituto de Catálisis y Petroleoquímica, CSIC.

(1) Boehm, E.; Bassant, J. M.; Steil, M. C.; Dordor, P.; Mauvy, F.; Grenier, J. C. *Solid State Ionics* **2003**, *5*, 973.
(2) Lang, Y.; Chen, C. L.; Chen, S. Y.; Chu, C. W.; Jacoboson, A. *J. Electrochem. Soc.* **2000**, *147* (11), 4001.
(3) Steele, B. C. H. *Proceedings of the 1st European SOFC Forum*U. Bossel: Lucerne, Switzerland,1994; Vol. 1, p 375.
(4) Bouwmeester, H. J. M.; Burgraaf, A. J. In *Fundamentals of Inorganic Membrane Science and Technology*; Burgraaf, A. J., Cot, L. Ž., Eds.; Elsevier: Amsterdam, The Netherlands, 1996; p 435.
(5) Fleig, J.; Maier, J. *J. Eur. Ceram. Soc.* **2004**, *24*, 1343.

10.1021/cm071837x CCC: $37.00
Published on Web 11/22/2007

From the pioneering work by Grenier et al. [6,7] and Takeda et al.,[8] it was established that $SrCoO_{3-\delta}$ oxides prepared at ambient-pressure conditions, in an air atmosphere, showed an approximate stoichiometry of $Sr_2Co_2O_5$ (or $SrCoO_{2.5}$) and adopted two very different structural types, with orthorhombic (the so-called high-temperature phase) or hexagonal (the low-temperature phase) symmetry. By quenching of the samples from the reaction temperature (1000 °C), an orthorhombic brownmillerite-type structure was obtained, showing alternating layers of CoO_4 tetrahedra and CoO_6 octahedra, sharing corners.[8] It belongs to the so-called 3C perovskite structural polytypes, characterized by a three-dimensional arrangement of corner-sharing polyhedra. By slow cooling of the $SrCoO_{3-\delta}$ sample in air, a hexagonal polytype is obtained, with a structure related to that of 2H-$BaNiO_3$,[6] characterized by a face-sharing arrangement of CoO_6 octahedra, as determined by Battle et al.[9–11] Further studies demonstrated that this low-temperature phase is, in fact, slightly Co-deficient, with a stoichiometry of $Sr_6Co_5O_{15}$.[12] At high temperatures, this hexagonal phase undergoes a transition to a cubic 3C structure.[13] If the synthesis is carried out under high-pressure conditions, the oxygen stoichiometry can be increased up to 3.0 in $SrCoO_3$, prepared at 6 GPa,[14,15] presenting a simple cubic 3C perovskite structure. Other Sr–Co–O oxides belonging to the Ruddlesden–Popper homologous series $Sr_{n+1}Co_nO_{3n+1}$ (n = 1–4) have also been reported[15] to be stabilized under high-pressure conditions.

From the point of view of their properties, high-temperature $SrCoO_{3-\delta}$ phases with 3C-like crystal structures are presented as mixed conductors with very high oxygen permeability. Among the various phase structures of $SrCoO_{3-\delta}$, the oxide with the cubic phase shows the highest electronic and oxygen ionic conductivity, with a maximum reported total electrical conductivity of ~160 $S \cdot cm^{-1}$ at ~950 °C.[16] It has also been observed that the oxygen permeability in related solid solutions increases with a decrease of the concentration of the substituting cations for Sr and Co.[17] However, the $SrCoO_{3-\delta}$ samples with 2H-like hexagonal structures at room temperature (RT) have shown to be almost non-oxygen-permeable.[18] Moreover, this hexagonal phase suffers from phase transitions when the sample is heated in air.[13] This phase transition provokes abrupt changes in the expansion coefficient that would led to cracking problems during the cell operation.

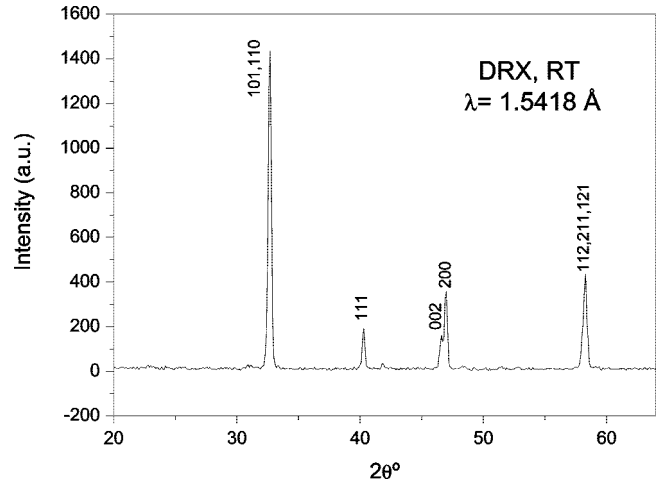

Figure 1. XRD diagram of $SrCo_{0.9}Sb_{0.1}O_{3-\delta}$, tentatively indexed in a simple tetragonal cubic unit cell with $a \sim 3.87$ Å and $c \sim 3.90$ Å.

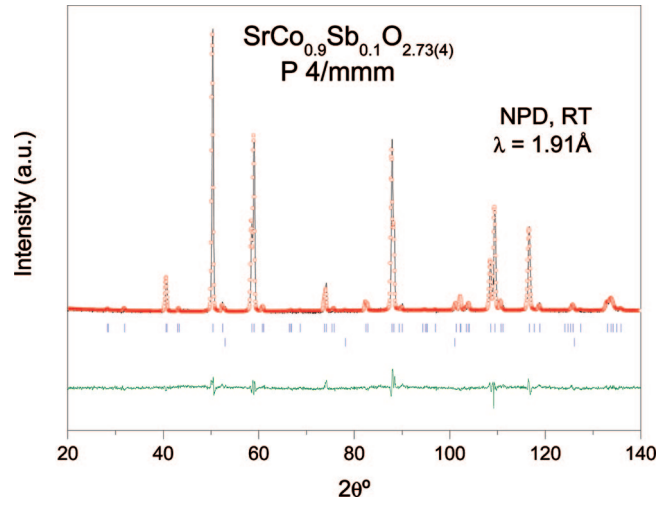

Figure 2. Observed (circles), calculated (full line), and difference (at the bottom) NPD profiles for $SrCo_{0.9}Sb_{0.1}O_{2.73(4)}$ at RT, refined in the *P4/mmm* space group. The second row of Bragg reflections correspond to vanadium from the sample holder.

The aim of the present work was the stabilization in the Sr–Co–O system of a cubic phase with a 3C-like crystal structure, with good properties as a mixed conductor to be used as a cathode material in IT-SOFCs. We present the results on the synthesis and characterization of a new perovskite of stoichiometry $SrCo_{0.9}Sb_{0.1}O_{3-\delta}$, studied by temperature-dependent neutron diffraction, thermal analysis, electrical transport, and thermal expansion measurements.

Experimental Section

$SrCo_{0.9}Sb_{0.1}O_{3-\delta}$ was synthesized via a nitrate–citrate route. Stoichiometric amounts of commercial Sb_2O_3, $SrNO_3$, and $Co(NO_3)_2 \cdot 6H_2O$ were dissolved in a citric acid aqueous solution containing some drops of HNO_3, under stirring. The solution was slowly evaporated, leading to an organic resin, which was dried at 120 °C and slowly decomposed at temperatures of up to 600 °C. The sample was then heated at 900 °C for 12 h and at 1000 °C for 24 h with intermediate grinding. After the thermal treatments, the sample was slow-cooled in the furnace.

(6) Grenier, J. C.; Ghodbane, S.; Demazeau, G.; Pouchard, M.; Hagenmuller, P. *Mater. Res. Bull.* **1979**, *14*, 831.
(7) Grenier, J. C.; Fournès, L.; Pouchard, M.; Hagenmuller, P. *Mater. Res. Bull.* **1986**, *21*, 441.
(8) Takeda, T.; Yamaguchi, Y.; Watanabe, H.; Tomiyoshi, S.; Yamamoto, H. *J. Phys. Soc. Jpn.* **1969**, *26*, 1320.
(9) Battle, P. D.; Gibb, T. C.; Steel, A. T. *J. Chem. Soc., Dalton Trans.* **1987**, 2359.
(10) Battle, P. D.; Gibb, T. C. *J. Chem. Soc., Dalton Trans.* **1987**, 667.
(11) Battle, P. D.; Gibb, T. C.; Steel, A. T. *J. Chem. Soc., Dalton Trans.* **1988**, 83.
(12) Harrison, W.; Hedwood, S. L.; Jacobson, A. J. *J. Chem. Soc., Chem. Commun.* **1995**, 1953.
(13) Rodríguez, J.; González Calbet, J. M.; Grenier, J. C.; Pannetier, J.; Anne, M. *Solid State Commun.* **1987**, *62* (4), 231.
(14) Taguchi, H.; Shimada, M.; Koizumi, M. *J. Solid State Chem.* **1979**, *29*, 221.
(15) Wang, X. L.; Sakurai, H.; Takayama-Muromachi, E. *J. Appl. Phys.* **2005**, *97*, 10M519.
(16) Deng, Z. Q.; Yang, W. S.; Liu, W.; Chen, C. S. *J. Solid State Chem.* **2006**, *179*, 362.
(17) Teraoka, Y.; Zhang, H. M.; Furukawa, S.; Yamazoe, N. *Chem. Lett.* **1985**, 1743.
(18) Kruidhof, H.; Bouwmeester, H. J. M.; Doorn, R. H. E. V.; Burggraaf, A. J. *Solid State Ionics* **1993**, *63–65*, 816.

Table 1. Unit-Cell, Positional, and Thermal Parameters for $SrCo_{0.9}Sb_{0.1}O_{3-\delta}$ in the Tetragonal *P4/mmm* (No. 123) Space Group, $Z = 2$, from NPD Data at RT and 300 and 500 °C and in the Cubic *Pm*$\bar{3}$*m* (No. 221) Space Group, $Z = 1$, at 700 and 940 °C

	RT	300 °C	500 °C	700 °C	940 °C
a (Å)	3.87694(8)	3.8941(1)	3.9174(1)	3.9446(1)	3.9702(1)
b (Å)	3.87694(8)	3.8941(1)	3.9174(1)	3.9446(1)	3.9702(1)
c (Å)	7.8134(2)	7.8301(2)	7.8732(3)	3.9446(1)	3.9702(1)
V (Å^3)	117.440(5)	118.737(5)	120.818(6)	61.380(3)	62.579(4)
		Sr 2h (½, ½, z)			Sr 1b (½, ½, ½)
z	0.2611(4)	0.2593(5)	0.2596(6)		
B (Å^2)	1.39(7)	1.57(9)	2.0 (1)	2.83(13)	3.28(14)
f_{occ}	1.0	1.0	1.0	1.0	1.0
		(Co,Sb)1 1a (0, 0, 0)			Co 1a (0, 0, 0)
B (Å^2)	0.4(2)	0.4(4)	0.8(4)	1.1(2)	1.6(2)
f_{occ}(Co)	0.9	0.9	0.9	0.9	0.9
		(Co,Sb)2 1b (0, 0, ½)			
B (Å^2)	0.9(3)	0.9(4)	0.9(4)		
f_{occ}(Co)	0.9	0.9	0.9		
		O1 2e (½, 0, 0)			O 3d (½, 0, 0)
B (Å^2)	1.1(1)	1.2(1)	1.6(2)	3.59(11)	4.53(12)
f_{occ}	1.0	1.0	1.0	0.863(1)	0.840(1)
		O2 2g (0, 0, z)			
z	0.7673(5)	0.7664(7)	0.7687(8)		
B (Å^2)	1.6(2)	2.0(2)	2.5(4)		
f_{occ}	0.91(2)	0.92(3)	0.90(4)		
		O3 2f (½, 0, ½)			
B (Å^2)	5.3[a]	4.7(2)	5.6(3)		
f_{occ}	0.82(2)	0.85(2)	0.82(2)		
		Reliability Factors			
χ^2	2.62	1.64	1.64	2.77	2.06
R_p (%)	5.66	2.93	2.93	3.57	3.32
R_{wp} (%)	7.29	3.75	3.72	4.66	4.05
R_{exp} (%)	4.50	2.93	2.90	2.80	2.83
R_{Bragg} (%)	6.05	6.85	7.49	5.87	8.24

[a] Anisotropic thermal factors: $\beta_{11} = 0.075(6)$, $\beta_{22} = 0.131(9)$, $\beta_{33} = 0.014(1)$; $\beta_{12} = \beta_{13} = \beta_{23} = 0$.

The reaction products were characterized by X-ray diffraction (XRD) for phase identification and for assessment of the phase purity. Neutron powder diffraction (NPD) data were collected at RT using the diffractometer D1A at ILL, Grenoble, France. The high-intensity mode ($\Delta d/d \leq 2 \times 10^{-3}$) was selected, with a neutron wavelength of $\lambda = 1.91$ Å within the angular 2θ range from 5° to 165°. Two grams of the sample was contained in a vanadium can for the RT measurement. The high-temperature measurements were carried out in air at intervals of 200 °C from 300 to 950 °C. For this purpose the sample was contained in a quartz tube open to ambient atmosphere, placed in the isothermal zone of a furnace with a vanadium resistor operating under vacuum ($P_{O_2} \approx 10^{-6}$ Torr). The collection time was of 3 h per pattern. Diffraction data were analyzed by the Rietveld method, using the *FULLPROF* program[19] with the use of its internal tables for scattering lengths. The line shape of the diffraction peaks was generated by a pseudo-Voigt function and the background refined to a fifth-degree polynomial. In the final run, the following parameters were refined: background coefficients (only for the RT data), zero-point, half-width, pseudo-Voigt, and asymmetry parameters for the peak shape, scale factor, and unit-cell parameters. For the NPD patterns collected above RT, the irregular background coming from the quartz container was interpolated from points devoid of reflections. Positional and occupancy factors for O atoms and isotropic thermal factors were also refined for NPD data. The coherent scattering lengths for Sr, Co, Sb, and O were 7.02, 2.49, 5.57, and 5.803 fm, respectively.

(19) Rodríguez-Carvajal, J. *Physica B* **1993**, *192*, 55.

Differential thermal analysis (DTA) and thermogravimetric analysis (TGA) curves in air were simultaneously obtained in a Stanton STA 781 instrument. The temperatures of the peaks were measured with an accuracy of ±1 °C. Analyses were carried out in still air at a 10 °C·min^{-1} heating/cooling rate. The sample and reference were situated in platinum crucibles, and α-Al_2O_3 was the inert reference. The TGA curve in reducing conditions was recorded in a Mettler-Toledo STAR SW 9.01 instrument, in the 30–900 °C temperature range, under a H_2 (10%)/N_2 (90%) flow (100 mL·min^{-1}). About 50 mg was used in each experiment.

For measurements of the thermal expansion and electrical conductivity, dense pellets are required. A pellet of $SrCo_{0.9}Sb_{0.1}O_{3-\delta}$ (10 mm in diameter and 1.4 mm thickness) was obtained by pressing the prepared powders under 1 ton of uniaxial pressure and sintered at 1200 °C for 5 h in air. A density of 70% of the crystallographic value was obtained under these conditions. The thermal expansion of the dense ceramic was studied using a Linseis L75/1550C dilatometer between 25 and 1000 °C in air with a heating rate of 5 °C·min^{-1}.

A direct current (dc) four-probe method was used for the electrical conductivity measurements from 25 to 1000 °C in air. For this purpose, the dense pellet was placed onto an alumina support and four equidistant platinum points were pressed onto the sample surface using a spring-loaded alumina tube. A current load of 0.5–1 A was applied by a dc dual-output power supply (E3646 A; Agilent Technologies) and the potential drop recorded by a Fluke 179 True root-mean-square multimeter.

Results and Discussion

Crystallographic Characterization. The oxide of nominal stoichiometry $SrCo_{0.9}Sb_{0.1}O_{3-\delta}$ was obtained as a well-crystallized powder; the laboratory XRD pattern was indexed as a subtle tetragonal distortion of a simple perovskite unit cell, with $a = b \sim 3.87$ Å and $c \sim 3.90$ Å, as shown in Figure 1. However, the NPD diagram collected at D1A at RT immediately showed the presence of superstructure peaks, which were successfully indexed with the *TREOR4*[20] program in a tetragonal unit cell with a doubled c axis, as $a = b \approx a_0$ and $c \approx 2a_0$ (a_0 stands for the simple cubic perovskite unit cell, ~3.9 Å). A pattern matching of the NPD profile in the *P4/mmm* (No. 123) space group allowed us to precisely determine the unit-cell parameters as $a = 3.87694(8)$ Å and $c = 7.8134(2)$ Å at RT and to assess the absence of systematic extinctions. A perovskite structural model was built in *P4/mmm* with Sr at 2h ($^1/_2$, $^1/_2$, z), Co, and Sb randomly distributed over the 1a (0, 0, 0) (labeled (Co,Sb)1) and 1b (0, 0, $^1/_2$) (labeled (Co,Sb)2) sites, and the three kinds of O atoms, O1 at 2f ($^1/_2$, 0, 0), O2 at 2g (0, 0, z), and O3 at 2e ($^1/_2$, 0, $^1/_2$). The refinement of the crystal structure with isotropic thermal factors for all of the atoms gave exceptionally high B values for O3 (≈5 Å^2), suspecting a large anisotropic component for the vibrations of this atom. The anisotropic thermal factors for O3 were thus refined. As a parallel approach, we have considered the possibility that O3 atoms partially occupy the large multiplicity 8f (x, y, $^1/_2$) positions, allowing a rotation of the CoO_6 octahedra within the *ab* plane; this refinement converges to [0.524(8), 0.050(4), $^1/_2$] positions, close to ($^1/_2$, 0, $^1/_2$), with large standard deviations and large thermal factors [3.6(3) Å^2], which does not seem very convincing. Therefore, we have preferred to keep the O3 anisotropic refinement hereafter.

In the final run, the occupancy factors for the three types of O atoms were also refined. For O1, the occupancy converged to a value slightly higher than unity [1.03(2)], which was set to 1. At RT, we obtained a crystallographic formula $Sr(Co_{0.9}Sb_{0.1})O_{2.73(4)}$. Because the peaks of vanadium coming from the sample holder were detected during the refinement, this metal was introduced as a second phase. Figure 2 illustrates the goodness of fit; Table 1 lists the final structural parameters and discrepancy factors obtained from RT NPD data.

Inspection of the NPD diagrams collected above RT shows that, at 300 and 500 °C, the structure keeps the mentioned tetragonal structure, which could be properly refined in spite of the irregular background coming from the quartz container; Table 1 also collects the structural parameters at 300 and 500 °C. Figure 3a illustrates the quality of the fit at 300 °C. Surprisingly, the NPD diagram collected at 700 °C showed the disappearance of the superstructure reflections arising from the doubling of the unit cell along the c direction; all of the peaks could be indexed in a simple cubic perovskite unit cell with $a = a_0$. The structure was modeled in the space group $Pm\bar{3}m$ with Sr at 1b ($^1/_2$, $^1/_2$, $^1/_2$) positions, Co and Sb distributed at random over the 1a (0, 0, 0) positions, and a single type of O atoms at 3d ($^1/_2$, 0, 0) sites. The structure was successfully refined at 700 and 940 °C; Figure 3b illustrates the goodness of the fit for the 700 °C diagram. Table 1 contains the main structural parameters of the cubic structures at 700 and 940 °C. Table 2 lists the main interatomic distances for the different temperatures.

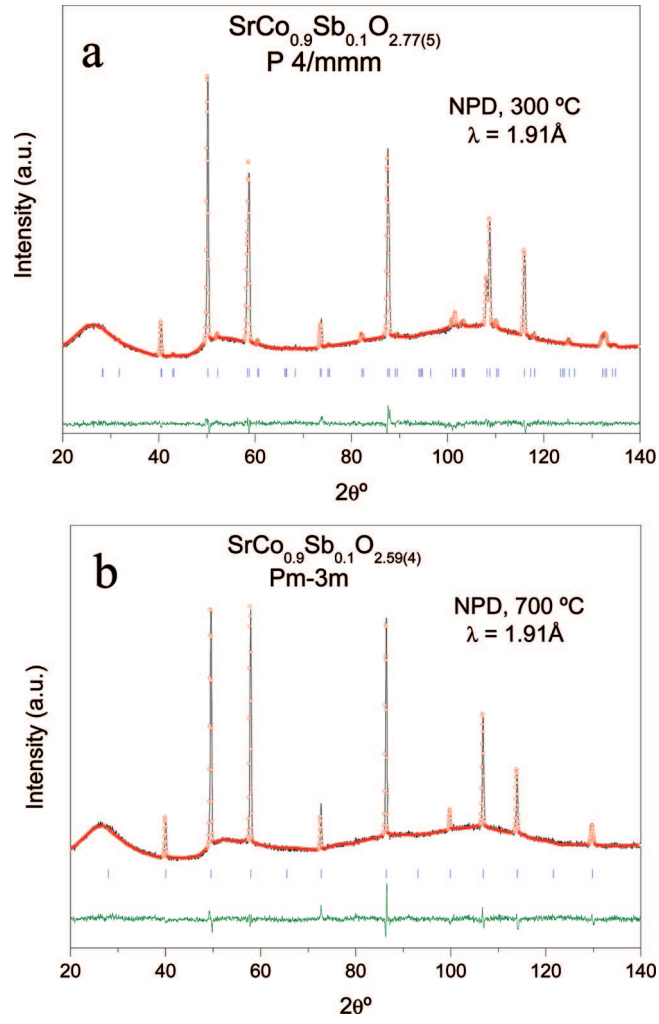

Figure 3. Rietveld plots for $SrCo_{0.9}Sb_{0.1}O_{3-\delta}$ refined from NPD data collected at (a) 300 °C (space group *P4/mmm*) and (b) 700 °C (space group $Pm\bar{3}m$). The irregular background is due to the quartz container.

Figure 4 displays the evolution of the unit-cell parameters in the studied temperature range, showing the transition from a low-temperature tetragonal superstructure to a high-temperature simple cubic symmetry. The undetermined transition temperature is in the 500–700 °C range.

Thermal Analysis. The oxygen content of the pristine sample was determined by thermal analysis under reducing conditions. Figure 5 shows the TGA and DTG curves of $SrCo_{0.9}Sb_{0.1}O_{3-\delta}$ obtained in a 10% H_2 flow. A weight loss of 14.19% is observed between 275 and 900 °C. A subsequent isothermal heating at 900 °C for 30 min allowed us to assess that the sample is fully decomposed at this temperature. After cooling of the sample, the final product was identified by XRD as a mixture of SrO, Co metal, and Sb_2O_3. From the observed weight loss, the oxygen stoichiometry of the starting sample is 2.72(2), in excellent agreement with that determined by neutron diffraction.

(20) Werner, P. E.; Eriksson, L.; Westdahl, M. *J. Appl. Crystallogr.* **1985**, *16*, 367.

Table 2. Main Bond Distances (Å) for Tetragonal and Cubic $SrCo_{0.9}Sb_{0.1}O_{3-\delta}$ Phases Determined from NPD Data at RT and 300, 500, 700, and 940 °C

P4/mmm	RT	300 °C	500 °C	*Pm*$\bar{3}$*m*	700 °C	940 °C
		SrO_{12} Polyhedron				SrO_{12} Polyhedron
Sr–O1 (×4)	2.814(2)	2.814(3)	2.831(3)	Sr–O (×12)	2.7893(1)	2.8073(1)
Sr–O2 (×4)	2.7504(4)	2.7609(5)	2.7789(6)			
Sr–O3 (×4)	2.691(2)	2.709(3)	2.723(3)			
⟨Sr–O⟩	2.758	2.767	2.778			
		$(Co,Sb)1O_6$ Octahedron				$(Co,Sb)1O_6$ Octahedron
(Co,Sb)1–O1 (×4)	1.9385(0)	1.9471(0)	1.9587(0)	(Co,Sb)–O (×6)	1.9723(1)	1.9851(1)
(Co,Sb)1–O2 (×2)	1.818(4)	1.830(5)	1.821(6)			
⟨(Co,Sb)1–O⟩	1.898	1.908	1.913			
		$(Co,Sb)2O_6$ Octahedron				
(Co,Sb)2–O2 (×2)	2.089(4)	2.085(5)	2.115(6)			
(Co,Sb)2–O3 (×4)	1.9385(0)	1.9471(0)	1.9587(0)			
⟨(Co,Sb)2–O⟩	1.989	1.993	2.011			

Figure 6 shows the thermal analysis and TGA and DTA curves for $SrCo_{0.9}Sb_{0.1}O_{3-\delta}$ carried out in air. In the temperature region where the phase transition tetragonal-to-cubic is expected (500–700 °C), there is no clear feature in the DTA curve that could correspond to this transition, except a broad exothermic band centered at about 600 °C; we conclude that the phase transition observed by diffraction methods involves a very small heat transfer because it corresponds to a subtle order–disorder transformation concerning the rearrangement of 0.26(4) oxygen vacancies per formula unit. By further heating of the sample, a sharp endothermic peak is observed at 913 °C, which in the cooling run appears as an exothermic peak at 790 °C. The origin of these peaks is uncertain; our NPD data at 940 °C do not show any additional transformation or any particular feature that cannot be understood on the basis of the simple cubic structural model. The TGA curve shows a weight loss, probably corresponding to oxygen release, starting at 450 °C and monotonously increasing up to 1000 °C. The oxygen loss at 940 °C (temperature of collection of the last NPD diagram) is 0.21(1) oxygen atoms per formula, and this process is virtually reversible. A XRD study of the sample after the thermal analysis experiment gives exactly the same diffraction pattern as that of the initial compound, confirming the absence of phase segregation or decomposition after the thermal treatment.

Electrical Transport and Thermal Expansion. The total conductivity (σ) of $SrCo_{0.9}Sb_{0.1}O_{3-\delta}$ was determined in air by the four-probe method in the temperature range 200–950 °C. Figure 7 shows an abrupt change of slope at about 400 °C, evolving from a positive, semiconducting-like slope to a negative slope, thus exhibiting a maximum conductivity of 300 $S \cdot cm^{-1}$ at this temperature. The electrical conductivity requirement for a SOFC cathode material is 100 $S \cdot cm^{-1}$ at the operating temperature. It is remarkable that the conductivity values obtained for this sample in the ordinary temperature interval in IT-SOFC (650–850 °C) are always higher than this value, even in a sample with a density of ~70%.

With the aim of determining the mechanical compatibility of $SrCo_{0.9}Sb_{0.1}O_{3-\delta}$ with the other cell components, thermal expansion measurements were carried out in air in the temperature range 25–1000 °C. Figure 8 shows a linear expansion without the presence of abrupt changes due to the absence of great structural changes in the phase transition detected in this temperature range. There is just a slight variation in the slope of the line at 400 °C (coincident with T_{MI}) and 650 °C. This last change of slope could be related to the structural phase transition observed from NPD data. The thermal expansion coefficients obtained from the slope of the line at different temperature ranges are summarized in Table 3. The values obtained are very close to those presented by other Co-based perovskite materials.[21]

Discussion

At RT, $SrCo_{0.9}Sb_{0.1}O_{2.73(4)}$ exhibits a tetragonal superstructure of perovskite with a doubled a_0 axis along the *c* direction, as displayed in Figure 9a. Co and Sb atoms occupy at random the *B* positions of the perovskite; there is no tilting of the $(Co,Sb)O_6$ octahedra. This superstructure could be the result of the long-range ordering of the oxygen vacancies along the *c* axis, in alternating layers with different occupancy factors, 0.92(2) for O2 and 0.82(2) for O3. Both O2 and O3 are the equatorial O atoms of the octahedra; there is no measurable deficiency concerning the axial O1 oxygen. In the tetragonal structure, there are two kinds of $(Co,Sb)O_6$ octahedra: Those related to (Co,Sb)1 are flattened along the *c* axial direction, displaying extremely short (Co,Sb)1–O1 distances, of 1.82 Å. By contrast, the $(Co,Sb)2O_6$ octahedra are elongated, with (Co,Sb)2–O3 bond lengths of 2.09 Å. In both cases, the four equivalent equatorial distances are 1.938 Å. The fact that the structure contains alternating small $[(Co,Sb)1O_6]$ and large $[(Co,Sb)2O_6]$ octahedra, with average ⟨Co,Sb)–O⟩ distances of 1.9 and 2.0 Å, respectively, suggests the possibility of a charge ordering between Co^{4+} and Co^{3+} cations. Because the average valence for Co is 3.3+, the charge-ordering hypothesis would imply an average oxidation state of $Co^{3.6+}$ at (Co,Sb)1 sites and Co^{3+} and (Co,Sb)2 positions, assuming a full charge disproportionation.

The O atoms with lowest occupancy factors (O3) also present abnormally large thermal factors, showing an anisotropic vibration with the long axis of the thermal ellipsoid directed along the [1, 0, 0] direction, as represented in Figure 9b. The equivalent isotropic thermal factor for O3, of ≈5.3 $Å^2$, is significantly large for a metal oxide at RT; this large value already suggests a great mobility for these partially occupied O atoms.

(21) Wang, S.; Zheng, R.; Suzuki, A.; Hashimoto, T. *Solid State Ionics* **2004**, *174*, 157.

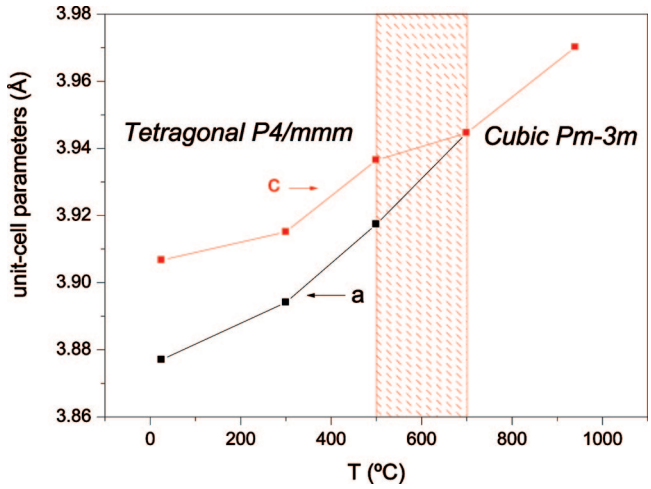

Figure 4. Unit-cell parameter variation with temperature for $SrCo_{0.9}Sb_{0.1}O_{3-\delta}$. A phase transition between tetragonal and cubic occurs between 500 and 700 °C.

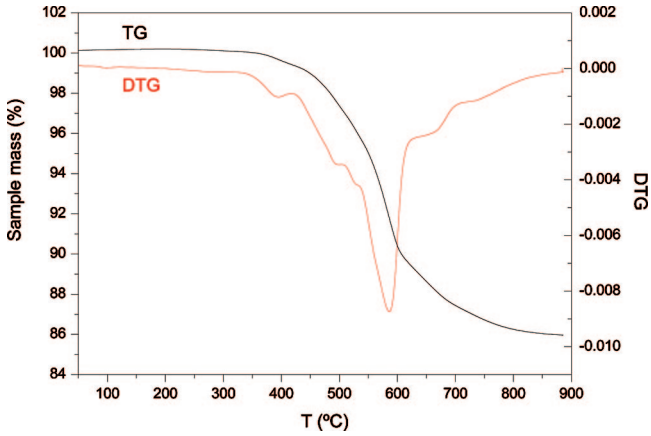

Figure 5. Thermal analysis under reducing conditions (10% H_2/90% N_2) of $SrCo_{0.9}Sb_{0.1}O_{3-\delta}$.

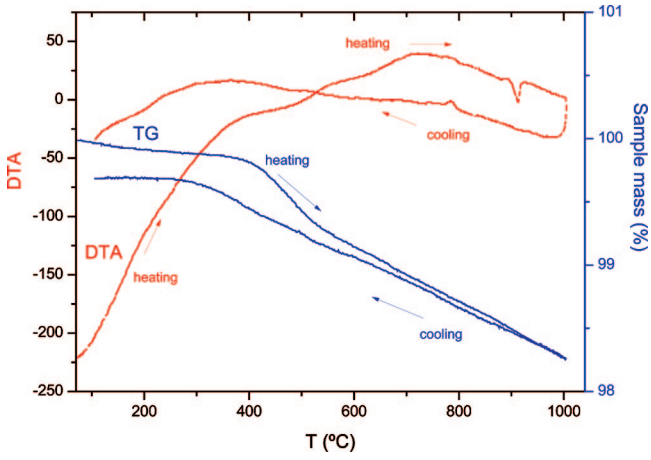

Figure 6. Thermal analysis curves collected in air for $SrCo_{0.9}Sb_{0.1}O_{3-\delta}$: TGA (left axis); DTA (right axis).

The observed phase transition undergone between 500 and 700 °C (probably at 650 °C, from thermal expansion data; Figure 8), from a tetragonal superstructure to a simple cubic perovskite, is clearly a nonreconstructive, second-order transition, involving a very small heat transfer giving no peaks at the DTA curve (Figure 6). This phase transition is related to the disordering of the oxygen vacancies over the

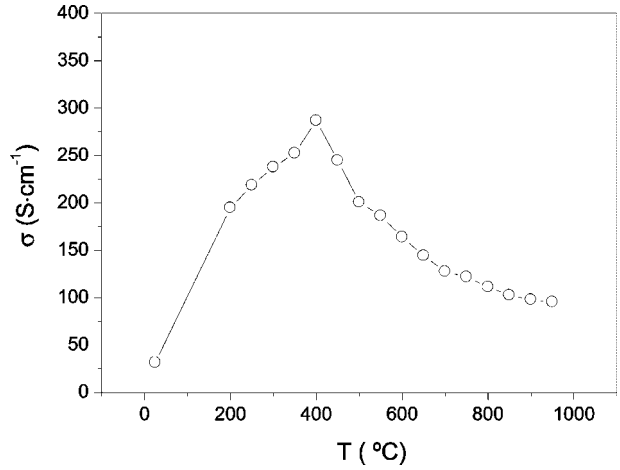

Figure 7. Total (electronic + ionic) conductivity in the temperature range from RT to 1000 °C for $SrCo_{0.9}Sb_{0.1}O_{3-\delta}$.

three available positions in the tetragonal structure, giving rise to a single oxygen site in the cubic unit cell with an average thermal factor and occupancy. Thus, the thermal factors for O1, O2, and O3 at 500 °C are respectively 1.6, 2.5, and 5.6 $Å^2$, merging into a single O atom with a isotropic B factor of 2.6 $Å^2$ at 700 °C.

The total oxygen content refined from NPD data slightly evolves from 2.73 atoms·fu^{-1} at RT to 2.72 atoms·fu^{-1} at 500 °C and then decreases to 2.59 and 2.52 atoms·fu^{-1} at 700 and 940 °C, respectively, showing a progressive oxygen loss of the sample, in equilibrium with an air atmosphere during the full NPD data acquisition. This is in good agreement with the weight loss observed in the TGA curve [0.21(1) O atoms per formula between RT and 940 °C]. By TGA, we observe that the sample is stable up to 450 °C, and then a progressive weight loss starts; by neutron diffraction, we observe a slight decrease of the oxygen contents at 500 °C and an abrupt mass loss at 700 °C, which is in overall agreement with the TGA observation, taking into account the error bars obtained from the neutron refinements, the possibly existing temperature shifts between both techniques, and the considerably more massive sample used in the neutron experiment, confined in a narrow quartz tube, which may have delayed in some way the oxygen release of the sample.

Assuming oxidation states of 2+ for Sr and 5+ for Sb, the average valence of Co cations evolves from 3.29+ at RT to 2.82+ at 940 °C. Connecting with the charge-ordering hypothesis, we suggest the appealing possibility that the phase transition to cubic is driven by the progressive reduction of the Co valence below to 3+, hence losing the charge-ordered 3+/4+ state. We could conclude that the melting of the low-temperature charge-ordered state is the driving force for the tetragonal to cubic transition.

The most interesting and novel issue of this paper is the stabilization of a new structural superstructutre of perovskite by the replacement of 10% Co by Sb in the $SrCoO_{3-\delta}$ perovskite. Under similar preparation conditions, a material with starting $SrCoO_{3-\delta}$ stoichiometry, prepared by slow cooling of the sample in air under ambient-pressure conditions, would have given a hexagonal 2H-like polytype

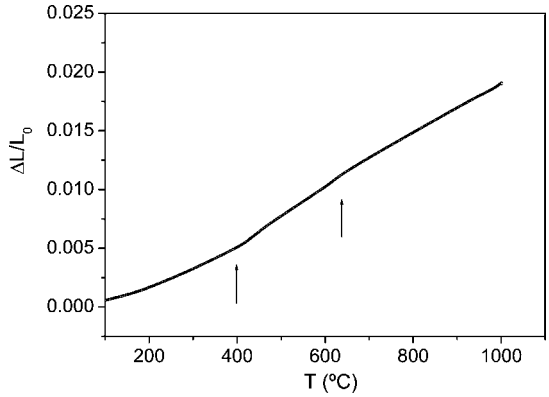

Figure 8. Thermal expansion curve collected in air in the temperature range from RT to 1000 °C for $SrCo_{0.9}Sb_{0.1}O_{3-\delta}$.

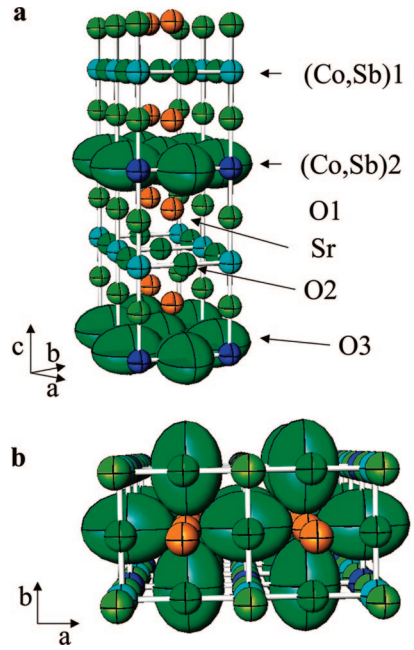

Figure 9. Two views of the tetragonal crystal structure observed for $SrCo_{0.9}Sb_{0.1}O_{3-\delta}$ between RT and 500 °C. (a) Array of corner-linked $(Co,Sb)O_6$ octahedra, with alternating layers of partially occupied O3 positions corresponding to O atoms with large, anisotropic (80% of probability) thermal factors. (b) Two unit cells projected along the *c* direction.

Table 3. Thermal Expansion Coefficients of $SrCo_{0.9}Sb_{0.1}O_{3-\delta}$ in Different Temperature Ranges

T (°C)	100–400	400–650	650–1000
TEC ($\times 10^{-6}$ K^{-1})	16.2	25.7	21.2

containing face-sharing octahedra. The electrical properties of this last material are very poor at moderate temperatures; however, the 2H polytype undergoes a high-temperature transition to a simple cubic phase above 900 °C,[13] with a corner-sharing 3C structure, characterized by a dramatic improvement in the total conductivity, from 20 $S \cdot cm^{-1}$ at RT to more than 160 $S \cdot cm^{-1}$ at 950 °C.[16] Unhappily, this temperature is too high for this $SrCoO_{3-\delta}$ oxide to find applications in IT-SOFCs, and furthermore the reconstructive 2H–3C transition undergone by $SrCoO_{3-\delta}$ above 900 °C is a serious drawback that would compromise the mechanical resistance of the material in the SOFC operating conditions. In the present work, the introduction of 10% Sb into the Co positions of the perovskite stabilizes a "pseudocubic" 3C-like phase from RT to 500 °C, which then undergoes a subtle, nonreconstructive transition between 500 and 700 °C to a cubic, disordered phase, exhibiting excellent conductivity values up 300 $S \cdot cm^{-1}$ at 400 °C. In the working range of a IT-SOFC (650–850 °C), the conductivity is well above 100 $S \cdot cm^{-1}$.

The stabilization of a 3C perovskite structure with corner-sharing CoO_6 octahedra by the introduction of 10% Sb atoms can be understood if we take into account that the presence of highly charged Sb^{5+} cations distributed at random over the *B* octahedral positions prevents the highly repulsive conformations derived from the octahedral face sharing involved in the hexagonal 2H polytypes; a corner-sharing configuration minimizes the mentioned repulsions. On the other hand, the introduction of Sb^{5+} cations drives an electron-doping effect, enhancing the mixed valence over the Co cations and promoting the electrical conductivity. Another recent approach[22] for the stabilization of the cubic phase is the introduction of large size cations at the Co positions: 5% of Sc, combined with a sol–gel synthesis procedure, led to a cubic perovskite phase, as assessed by XRD, with a maximum conductivity, in air, of 177 $S \cdot cm^{-1}$.[22]

Finally, it is worth underlying that the thermal expansion of $SrCo_{0.9}Sb_{0.1}O_{3-\delta}$ is virtually linear, without the presence of abrupt changes that could be detrimental for the mechanical stability of any electrochemical device. The change of slope observed at 400 °C (Figure 8) coincides with the abrupt change observed in the dc electrical conductivity (Figure 7); similar variations have also been reported by other authors in $LaCoO_{3-\delta}$ materials[23] (also containing Co^{3+} cations) and related to a change in the state of the e_g electrons that become itinerant in the metallic state, promoting subtle variations on the lattice parameters and, hence, on the thermal expansion. The second change in the slope of the linear expansion (Figure 8), observed around 650 °C, could be related to the tetragonal to cubic transition observed by means of NPD, as already mentioned.

Conclusions

$SrCo_{0.9}Sb_{0.1}O_{2.73(4)}$ presents a tetragonal superstructure of perovskite in the temperature range from RT to 500 °C, consisting of an untilted corner-sharing arrangement of elongated and flattened octahedra alternating along the *c* direction. The oxygen deficiency is concentrated in the equatorial O atoms, characterized by large thermal factors, suggesting a significant ionic mobility. This phase undergoes a transition to a completely disordered structure, described in a simple cubic perovskite unit cell, in the temperature range 500–700 °C, probably at 650 °C from thermal expansion measurements. This structure is stable up to 940 °C; at this temperature, the oxygen stoichiometry is 2.52(4). This order–disorder, nonreconstructive phase transition is not detected at the DTA curves; because this transition does not involve an abrupt change in the cell volume, the thermal

(22) Zeng, P.; Ran, R.; Chen, Z.; Zhou, W.; Gu, H.; Shao, Z.; Liu, S. *J. Alloys Compd.* **2007**,in press. Doi: 10.1016/j.jallcom.2007.01.144.
(23) Uhlenbruck, S.; Tietz, F. *Mater. Sci. Eng.* **2004**, *B107*, 277.

expansion smoothly increases in all of the temperature interval up to 1000 °C. The total conductivity displays a maximum value of 300 $S \cdot cm^{-1}$ at 400 °C and then smoothly decreases, always presenting values substantially above the required 100 $S \cdot cm^{-1}$, in the working regime of IT-SOFCs between 650 and 850 °C.

Acknowledgment. We are thankful for the financial support of Spanish CICyT (Project MAT2004-0479 and MAT2005-02933) and of "Comunidad de Madrid" (Project ENERCAM-CM S-0505/ENE/0304). We are grateful to ILL for making all of the facilities available.

CM071837X